DOI 10.1007/s10946-024-10182-w
Journal of Russian Laser Research, Volume 45, Number 1, January, 2024

PROBABILITY REPRESENTATION OF NONCLASSICAL STATES OF THE INVERTED OSCILLATOR

Matyas Mechler,[1,2] Margarita A. Man'ko,[3*] Vladimir I. Man'ko,[3] and Peter Adam[1,2]

[1] *Institute for Solid State Physics and Optics, HUN-REN Wigner Research Centre for Physics P.O. Box 49, Budapest H-1525, Hungary*

[2] *Institute of Physics, University of Pécs Ifjúság útja 6, Pécs H-7624, Hungary*

[3] *Lebedev Physical Institute, Russian Academy of Sciences Leninskii Prospect 53, Moscow 119991, Russia*

*Corresponding author e-mail: mankoma@lebedev.ru

Abstract

We determine the evolving probability representations of several important nonclassical states of the inverted oscillator by applying the method of integrals of motion for this system. The considered nonclassical states initially prepared in the potential of the harmonic oscillator are even and odd Schrödinger cat states, squeezed coherent states, and lattice superpositions of coherent states. The latter superpositions can approximate several nonclassical states with high precision, hence their probability representation can describe various nonclassical states of the inverted oscillators. Explicit results are shown for the approximation of number states, photon number superpositions, and amplitude squeezed states by determining the parameters of the superposition appearing in the probability

Keywords: nonclassical states, inverted oscillator, probability representation, symplectic tomogram.

1. Introduction

Recently, the probability representation of quantum mechanics was constructed, where the system states were described by conventional nonnegative probability distributions defined in the phase space [1–5]. This representation can be derived from the density operator, and it contains all information on the quantum system. In the probability representation, all quantum effects can be effectively explained applying the standard properties of the conventional probability theory. The probability representation is connected with other known quasiprobability representations, such as the Wigner function [6], the Husimi Q-function [7,8], and the Glauber–Sudarshan P-function [9,10] by integral transforms [11]. The idea of probability representation has been extended to discrete spin variables [12–21]. General formalism describing all invertible maps connecting operators acting in a Hilbert space and functions of some variables has also been developed [22].

Probability representations known as symplectic tomograms have been derived for several important states of the harmonic oscillator, including coherent states, Fock states [5], thermal states [23], and Schrödinger cat states [24] originally introduced as even and odd coherent states [25]. The evolution of these initial tomograms has been also derived, using the method of integrals of motion for systems, where these integrals of motion are linear in the position and momentum operators, e.g., for free particle motion [3,5,23].

Manuscript submitted by the authors in English on January 25, 2024.

The inverted harmonic oscillator, where the potential energy corresponds to imaginary frequencies of the oscillator, was recently considered in relation to cosmological problems [26–28]. Some other problems of the inverted oscillator were also discussed in Refs. [29–32]. Tomograms of evolving coherent and Fock states of the inverted oscillator, initially prepared in the potential of the usual harmonic oscillator, were derived in Ref. [33]. The evolution of even and odd Schrödinger cat states of the two-mode inverted oscillator has also been obtained in the center-of-mass tomographic probability description [34].

In this paper, we consider the evolution of even and odd Schrödinger cat states, squeezed coherent states, and lattice superpositions of coherent states of the inverted oscillator in the probability representation. We determine the evolving symplectic tomograms of these nonclassical states of the inverted oscillator, applying the method developed in Refs. [23,33] for obtaining the evolving probability distribution from the initial probability distribution, that is, from the tomograms of the considered nonclassical states initially prepared in the potential of the harmonic oscillator. The lattice superpositions of coherent states can approximate several nonclassical states with high precision, hence their tomograms can describe various nonclassical states of the inverted oscillators. We show examples for the approximation of number states, photon number superpositions, and amplitude squeezed states by determining the parameters of the superposition.

This paper is organized as follows.

In Sec. 2, we review the construction of probability representation of quantum states. In Sec. 3, we present our results on the evolution of symplectic tomograms of the considered nonclassical states of the inverted oscillator. Finally, the results obtained are discussed in Sec. 4.

2. Probability Representation of Quantum States

Any function representing quantum states in the phase space can be derived, using the general method introduced in Ref. [22]. In this formalism, all invertible maps, connecting operators acting in the Hilbert space $\mathcal{H}$, and functions of some variables can be described by two sets of operators called dequantizers $\hat{U}(\bar{x})$ and quantizers $\hat{D}(\bar{x})$. The vector $\bar{x} = (x_1, x_2, \ldots, x_n)$ labels the particular operators in the set. The parameters x_i can be either continuous or discrete ones. One can construct a function $f_A(\bar{x})$, called symbol of the operator $\hat{A}$, using the definition

$$f_A(\bar{x}) = \mathrm{Tr}(\hat{A}\hat{U}(\bar{x})). \tag{1}$$

The operator $\hat{A}$ can be expressed in terms of symbol of the operator as

$$\hat{A} = \int f_A(\bar{x})\hat{D}(\bar{x})\,\mathrm{d}\bar{x}, \tag{2}$$

in the case of continuous parameters x_i. We note that, in the case of discrete variables x_i, the integral in this equation should be replaced by a corresponding sum. All these expressions are valid for density operators $\hat{\rho}$.

According to this formalism, the density operator $\hat{\rho}$ can be mapped onto the function $w(X|\mu,\nu)$, called symplectic tomogram, by the following expression:

$$w(X|\mu,\nu) = \mathrm{Tr}\left[\hat{\rho}\,\delta\left(X\hat{\mathbf{1}} - \mu\hat{q} - \nu\hat{p}\right)\right], \tag{3}$$

with $\hat{q}$ and $\hat{p}$ being the position and momentum operators, respectively. Here, the dequantizer operator reads $\hat{U}(X,\mu,\nu) = \delta\left(X\hat{\mathbf{1}} - \mu\hat{q} - \nu\hat{p}\right)$. The function $w(X|\mu,\nu)$ is a nonnegative conditional probability distribution function of random position X satisfying the normalization condition

$$\int w(X|\mu,\nu)\,\mathrm{d}X = 1. \tag{4}$$

The conditions are labeled by parameters μ and ν determining the reference frames, where the position X is measured (i.e., the position X is determined as $X = \mu q + \nu p$ in the reference frame in the phase space).

The inverse transform reads

$$\hat{\rho} = \frac{1}{2\pi}\int w(X|\mu,\nu)\exp\left[i\left(X\hat{\mathbf{1}} - \mu\hat{q} - \nu\hat{p}\right)\right]\,\mathrm{d}X\,\mathrm{d}\mu\,\mathrm{d}\nu. \tag{5}$$

Hence, the quantizer operator is $\hat{D}(X,\mu,\nu) = \dfrac{1}{2\pi}\exp\left[i(X\hat{\mathbf{1}} - \mu\hat{q} - \nu\hat{p})\right]$.

For pure states, $\hat{\rho} = |\psi\rangle\langle\psi|$, Eq. (3) can be converted into the expression

$$w(X|\mu,\nu) = \frac{1}{2\pi|\nu|}\left|\int \psi(y)\exp\left(\frac{i\mu}{2\nu}y^2 - \frac{iX}{\nu}y\right)\,\mathrm{d}y\right|^2, \tag{6}$$

where $\psi(y)$ is the wave function of the state.

Equation (3) is actually the quantum version of the Radon transform [35] of the probability density of two random variables $f(q,p)$ that can be written as

$$w_{\mathrm{cl}}(X|\mu,\nu) = \int f(q,p)\delta(X - \mu q - \nu p)\,\mathrm{d}q\,\mathrm{d}p. \tag{7}$$

The inverse Radon transform reads

$$f(q,p) = \frac{1}{4\pi^2}\int w_{\mathrm{cl}}(X|\mu,\nu)e^{i(X-\mu q-\nu p)}\,\mathrm{d}X\,\mathrm{d}\mu\,\mathrm{d}\nu. \tag{8}$$

The relations (7) and (8) provide the invertible map of the probability density $f(q,p)$ onto the conditional probability density $w_{\mathrm{cl}}(X|\mu,\nu)$ of one random position X, measured in a reference frame defined by the parameters μ and ν, i.e., onto the tomogram describing the classical state. The quantum tomogram given by (3) complies with the Heisenberg uncertainty relation, while the classical tomogram violates it. In view of this fact, the classical and quantum Radon transforms enable the derivation of probability distributions with properties corresponding to classical and quantum properties of the state, respectively.

We note that for a wave function, which is a normalized superposition of normalized wave functions, i.e., $\psi(y) = \sum_k c_k\psi_k(y)$, one has a probability distribution $w_\psi(X|\mu,\nu)$, which can be expressed as a superposition of the scalar products $\langle\psi_k|\hat{U}(X,\mu,\nu)|\psi_{k'}\rangle$; see Eq. (3). In this case, the application of Eq. (6) provides a tomogram $w_\psi(X|\mu,\nu)$ that can never be obtained for classical systems, as it describes quantum superposition. We also note that for the extension of this theory to multi-mode oscillators, entangled probability distributions can be introduced, which correspond to the description of entangled quantum states [34]. Such distributions have not been discussed in the classical probability theory.

The Wigner function, which is a quasiprobability distribution function in the phase space, is expressed in terms of the wave function as follows ($\hbar = 1$):

$$W(q,p) = \frac{1}{2\pi}\int \psi(q+u/2)\psi^*(q-u/2)\exp(-ipu)\,\mathrm{d}u. \tag{9}$$

In the general case, which includes mixed states, the Wigner function can be derived from the density matrix as

$$W(q,p) = \frac{1}{2\pi}\int_{-\infty}^{\infty} \langle q-u/2|\hat{\rho}|q+u/2\rangle e^{ipu}\,\mathrm{d}u, \tag{10}$$

where $\langle y||\psi\rangle = \psi(y)$. The Wigner function can be obtained from the symplectic tomogram as

$$W(q,p) = \frac{1}{2\pi}\int w(X|\mu,\nu)e^{i(X-\mu q-\nu p)}\,\mathrm{d}X\,\mathrm{d}\mu\,\mathrm{d}\nu. \tag{11}$$

The expression of the symplectic tomogram in terms of the Wigner function reads

$$w(X|\mu,\nu) = \frac{1}{2\pi}\int W(q,p)\delta(X-\mu q-\nu p)\,\mathrm{d}q\,\mathrm{d}p. \tag{12}$$

We note that, for $\mu = \cos(\theta)$ and $\nu = \sin(\theta)$, the symplectic tomogram yields the optical tomogram $w(X|\theta)$. This tomogram of photon states is measured in the experiments in quantum optics [36], and it is used to reconstruct the Wigner function [37–39].

In view of the previous expressions, the symplectic tomogram and the Wigner function contain all information on the density operator, that is, they completely describe the quantum state. Recall that symplectic tomograms are always nonnegative functions, hence they are usual probability distributions. In contrast, Wigner function can and normally does take on negative values for certain states, and this property is a usual indicator of quantum interference.

Finally, let us consider the time evolution of symplectic tomograms. The density operator $\hat{\rho}(t)$ of the system described with the Hamiltonian $\hat{H}$ evolves as

$$\hat{\rho}(t) = \hat{u}(t)\hat{\rho}(0)\hat{u}^\dagger(t), \tag{13}$$

where $\hat{u}(t) = \exp(-it\hat{H})$ is the time evolution operator. The tomogram $w(X|\mu,\nu,t)$, which corresponds to the density operator $\hat{\rho}(t)$, reads

$$w(X|\mu,\nu,t) = \mathrm{Tr}(\hat{\rho}(t)\delta(X\hat{\mathbf{1}} - \mu\hat{q} - \nu\hat{p})). \tag{14}$$

Using the properties of the trace of product of operators, we obtain

$$w(X|\mu,\nu,t) = \mathrm{Tr}(\hat{\rho}(0)\delta(X\hat{\mathbf{1}} - \mu\hat{q}_H(t) - \nu\hat{p}_H(t))) = w_0(X|\mu_H(t),\nu_H(t)), \tag{15}$$

where $\hat{q}_H(t)$ and $\hat{p}_H(t)$ are the position and momentum operators in the Heisenberg representation, that is,

$$\hat{q}_H(t) = \hat{u}^\dagger(t)\hat{q}\hat{u}(t), \qquad \hat{p}_H(t) = \hat{u}^\dagger(t)\hat{p}\hat{u}(t). \tag{16}$$

The Hamiltonian of the inverted oscillator, assuming $m = 1$, $\omega = 1$, and $\hbar = 1$, reads

$$\hat{H} = \frac{\hat{p}^2}{2} - \frac{\hat{q}^2}{2}. \tag{17}$$

For this system, the operators $\hat{q}_H(t)$ and $\hat{p}_H(t)$ can be obtained as

$$\hat{q}_H(t) = \hat{q}\cosh t + \hat{p}\sinh t, \tag{18}$$
$$\hat{p}_H(t) = \hat{q}\sinh t + \hat{p}\cosh t. \tag{19}$$

Using these expressions, the argument of the delta function in Eq. (15) can be written in the form

$$X\hat{\mathbf{1}} - \mu_H(t)\hat{q} - \nu_H(t)\hat{p} = X\hat{\mathbf{1}} - \mu\hat{q}_H(t) - \nu\hat{p}_H(t), \tag{20}$$

where

$$\mu_H(t) = \mu\cosh t + \nu\sinh t, \tag{21}$$
$$\nu_H(t) = \mu\sinh t + \nu\cosh t. \tag{22}$$

In this end, the symplectic tomogram $w(X|\mu,\nu,t)$ for the inverted oscillator can be obtained by substituting Eqs. (21) and (22) into Eq. (15).

3. Results

In this section, we derive the symplectic tomograms of evolving nonclassical states of the inverted oscillator initially prepared in the potential of the harmonic oscillator. The considered nonclassical states are Schrödinger cat states, squeezed coherent states, and lattice superpositions of coherent states. These latter superpositions can approximate several nonclassical states with high precision. We show examples for the approximation of number states, photon number superpositions, and amplitude squeezed states.

Even and odd Schrödinger's cat states are superpositions of two coherent states defined as

$$|\psi_{\alpha,\pm}\rangle = C_\pm(|\alpha,t\rangle \pm |-\alpha,t\rangle), \tag{23}$$

where

$$C_\pm = \frac{1}{\sqrt{2\left(1 \pm e^{-2|\alpha|^2}\right)}}. \tag{24}$$

Here, the positive sign refers to even cat states, while the negative sign corresponds to odd cat states. These states are frequently referred to as even and odd coherent states. The wave functions of these states read

$$\psi_{\alpha,\pm}(x) = \frac{1}{\sqrt{2\sqrt{\pi}[\exp(2\,\mathrm{Re}(\alpha)^2) \pm \exp(-2\,\mathrm{Im}(\alpha)^2])}}\left[\exp\left(\sqrt{2}\,\alpha x - \frac{x^2}{2}\right) \pm \exp\left(-\sqrt{2}\,\alpha x - \frac{x^2}{2}\right)\right]. \tag{25}$$

Substitution of the wave function (25) into Eq. (6) leads to the symplectic tomogram

$$w_{\alpha,\pm}(X|\mu,\nu) = \frac{1}{\sqrt{\sigma}\sqrt{\pi}N_\pm^2(\alpha)}\exp\left[\frac{-X^2-\overline{X}^2}{\sigma}\right]\left\{\exp\left[\frac{2X\overline{X}}{\sigma}\right] + \exp\left[\frac{-2X\overline{X}}{\sigma}\right] \pm 2\cos\left[\frac{2^{3/2}X(\mu\,\mathrm{Im}(\alpha) - \nu\,\mathrm{Re}(\alpha))}{\sigma}\right]\right\}, \tag{26}$$

where

$$\sigma = \mu^2 + \nu^2, \tag{27}$$
$$N_{\pm}^2(\alpha) = 2\left[1 \pm \exp(-2\left(\mathrm{Re}\,(\alpha)^2 + \mathrm{Im}\,(\alpha)^2\right))\right], \tag{28}$$

and the mean value of the random variable $\overline{X}$ reads

$$\overline{X} = \sqrt{2}(\mu\,\mathrm{Re}(\alpha) + \nu\,\mathrm{Im}(\alpha)). \tag{29}$$

Applying Eq. (15) and substituting Eqs. (21) and (22), we obtain the evolution of symplectic tomogram for the inverted oscillator as follows:

$$\begin{aligned} w_{\alpha,\pm}(X|\mu,\nu,t) = {} & \frac{1}{\sqrt{\sigma}\sqrt{\pi}N_{\pm}^2(\alpha)} \exp\left[\frac{-X^2 - 2\left[(\mathrm{Re}\,(\alpha)\nu + \mathrm{Im}\,(\alpha)\mu)\sinh t + (\mathrm{Re}\,(\alpha)\mu + \mathrm{Im}\,(\alpha)\nu)\cosh t\right]^2}{\sigma}\right] \\ & \times \left\{\exp\left[\frac{2^{3/2}X\left[\mathrm{Re}\,(\alpha)\left(\nu\sinh t + \mu\cosh t\right) + \mathrm{Im}(\alpha)\left(\nu\cosh t + \mu\sinh t\right)\right]}{\sigma}\right]\right. \\ & + \exp\left[\frac{-2^{3/2}X\left[\mathrm{Re}\,(\alpha)\left(\nu\sinh t + \mu\cosh t\right) + \mathrm{Im}\,(\alpha)\left(\nu\cosh t + \mu\sinh t\right)\right]}{\sigma}\right] \\ & \left. \pm\, 2\cos\left[\frac{2^{3/2}X\left[\mathrm{Im}\,(\alpha)\left(\nu\sinh t + \mu\cosh t\right) + \mathrm{Re}\,(\alpha)\left(\nu\cosh t + \mu\sinh t\right)\right]}{\sigma}\right]\right\}, \end{aligned} \tag{30}$$

where

$$\sigma = (\mu^2 + \nu^2)\cosh(2t) + 2\mu\nu\sinh(2t), \tag{31}$$
$$N_{\pm}^2(\alpha) = 2\left\{1 \pm \exp[-2\left(\mathrm{Re}(\alpha)^2 + \mathrm{Im}\,(\alpha)^2\right)]\right\}. \tag{32}$$

Squeezed coherent states can be obtained by applying the displacement and squeezing operators onto the vacuum state, that is,

$$|\zeta,\alpha\rangle = \hat{D}(\alpha)\hat{S}(\zeta)|0\rangle. \tag{33}$$

The displacement and squeezing operators are defined as

$$\hat{D}(\alpha) = \exp(\alpha\hat{a}^\dagger - \alpha^*\hat{a}), \qquad \hat{S}(\zeta) = \exp\left[\frac{1}{2}(\zeta^*\hat{a}^2 - \zeta(\hat{a}^\dagger)^2)\right], \tag{34}$$

where $\zeta = re^{i\phi}$, and r is the squeezing parameter. The wave function of the state $|\zeta,\alpha\rangle$ reads [40]

$$\begin{aligned} \psi_{\xi,\alpha}(x) = {} & \left(\frac{1}{\pi}\right)^{1/4} \frac{1}{\sqrt{|\cosh r - e^{i\phi}\sinh r|}} \frac{\sqrt{\cosh r - e^{-i\phi}\sinh r}}{\sqrt{|\cosh r - e^{-i\phi}\sinh r|}} \\ & \times \exp\left[-i\,\mathrm{Re}(\alpha)\,\mathrm{Im}(\alpha)\right] \exp\left[i\sqrt{2}\,\mathrm{Im}(\alpha)x\right] \\ & \times \exp\left[-\frac{\cosh r + e^{i\phi}\sinh r}{2(\cosh r - e^{i\phi}\sinh r)}(x - \sqrt{2}\,\mathrm{Re}(\alpha))^2\right]. \end{aligned} \tag{35}$$

Again, by substituting the wave function (35) into Eq. (6), we can obtain symplectic tomogram

$$w_{\xi,\alpha}(X|\mu,\nu) = \frac{1}{2\sqrt{\pi}} \frac{1}{\sqrt{\sinh(2r)\left[(\nu^2-\mu^2)\cos\phi - 2\mu\nu\sin\phi\right] + \cosh(2r)(\nu^2+\mu^2)}} \times \exp\left\{ \frac{-(\sqrt{2}\,\mathrm{Im}(\alpha)\nu + \sqrt{2}\,\mathrm{Re}(\alpha)\mu - X)^2}{\sinh(2r)\left[(\nu^2-\mu^2)\cos(\phi) - 2\mu\nu\sin(\phi)\right] + \cosh(2r)(\nu^2+\mu^2)} \right\}. \tag{36}$$

Then, the evolution of symplectic tomogram for the inverted oscillator can be obtained by substituting Eqs. (21) and (22); it reads

$$\begin{aligned} w_{\xi,\alpha}(X|\mu,\nu,t) = \frac{1}{2\sqrt{\pi}} &\left\{ \cosh(2r)\left[\cosh(2t)(\nu^2+\mu^2) + 2\sinh(2t)\mu\nu\right] \right. \\ &+ \sinh(2r)\left[(\nu^2-\mu^2)\cos\phi - \left(\sinh(2t)(\nu^2+\mu^2) + 2\cosh(2t)\mu\nu\right)\sin\phi\right] \Big\}^{-1/2} \\ &\times \exp\Big[-(\sqrt{2}\,\mathrm{Im}(\alpha)(\mu\sinh t + \nu\cosh t) + \sqrt{2}\,\mathrm{Re}(\alpha)(\mu\cosh t + \nu\sinh t) - X)^2 \\ &\times \Big(\cosh(2r)\left[\cosh(2t)(\nu^2+\mu^2) + 2\sinh(2t)\mu\nu\right] \\ &+ \sinh(2r)\left\{(\nu^2-\mu^2)\cos\phi - \left[\sinh(2t)(\nu^2+\mu^2) + 2\cosh(2t)\mu\nu\right]\sin\phi\right\}\Big)^{-1} \Big]. \end{aligned} \tag{37}$$

Finally, let us consider the superposition of nine coherent states

$$\left|\psi_9^{\mathrm{lattice}}\right\rangle = \sum_{l=-1}^{1}\sum_{k=-1}^{1} c_{k,l}|l\cdot d + k\cdot id\rangle \tag{38}$$

on an equidistant lattice centered around the origin in the phase space. In this equation, d denotes the distance between adjacent elements of the lattice, and $c_{k,l}$ are complex coefficients. Note that the coefficients $c_{k,l}$ are chosen so that the state $\left|\psi_9^{\mathrm{lattice}}\right\rangle$ is normalized. The corresponding wave function can be written as

$$\psi_9^{\mathrm{lattice}}(x) = \sum_{l=-1}^{1}\sum_{k=-1}^{1} c_{k,l}\frac{1}{\pi^{1/4}}\exp\left[-d^2(l^2+ikl) - \frac{x^2}{2} + \sqrt{2}(l\cdot d + k\cdot id)x\right]. \tag{39}$$

Then, by substituting the wave function (39) into Eq. (6), the resulting formula gives

$$\begin{aligned} w_9^{\mathrm{lattice}}(X|\mu,\nu) = &\frac{1}{\sqrt{\pi}\sqrt{\nu^2+\mu^2}} \\ \times &\left| \sum_{l=-1}^{1}\sum_{k=-1}^{1} c_{k,l}\exp[-d^2(l^2+ikl)]\exp\left(\frac{-i(\sqrt{2}(-ild+kd) - X/\nu)^2}{2(\mu/\nu+i)}\right)\right|^2, \end{aligned} \tag{40}$$

or, by calculating the absolute square in the formula, we arrive at

$$
\begin{aligned}
w_9^{\text{lattice}}(X|\mu,\nu) =& \frac{1}{\sqrt{\pi}\sqrt{\nu^2+\mu^2}} \times \left(\left\{ \sum_{l=-1}^{1} \sum_{k=-1}^{1} e^{-\frac{\left[\sqrt{2}d(k\nu+l\mu)-X\right]^2}{2(\nu^2+\mu^2)}} \right. \right. \\
& \times \left[\mathrm{Re}\,(c_{k,l}) \cos\left(\frac{2d^2\nu(k\nu+l\mu)(l\nu-k\mu)+2^{3/2}Xd\nu(k\mu-l\nu)-X^2\mu}{2\nu(\nu^2+\mu^2)} \right) \right. \\
& \left. \left. -\mathrm{Im}\,(c_{k,l}) \sin\left(\frac{2d^2\nu(k\nu+l\mu)(l\nu-k\mu)+2^{3/2}Xd\nu(k\mu-l\nu)-X^2\mu}{2\nu(\nu^2+\mu^2)} \right) \right] \right\}^2 \\
& + \left\{ \sum_{l=-1}^{1} \sum_{k=-1}^{1} e^{-\frac{\left[\sqrt{2}d(k\nu+l\mu)-X\right]^2}{2(\nu^2+\mu^2)}} \right. \\
& \times \left[\mathrm{Re}\,(c_{k,l}) \sin\left(\frac{2d^2\nu(k\nu+l\mu)(l\nu-k\mu)+2^{3/2}Xd\nu(k\mu-l\nu)-X^2\mu}{2\nu(\nu^2+\mu^2)} \right) \right. \\
& \left. \left. \left. +\mathrm{Im}\,(c_{k,l}) \cos\left(\frac{2d^2\nu(k\nu+l\mu)(l\nu-k\mu)+2^{3/2}Xd\nu(k\mu-l\nu)-X^2\mu}{2\nu(\nu^2+\mu^2)} \right) \right] \right\}^2 \right). \qquad (41)
\end{aligned}
$$

The evolution of symplectic tomogram for the inverted oscillator can be obtained, similarly to the previous cases, by substituting Eqs. (21) and (22); that leads to

$$
\begin{aligned}
w_9^{\text{lattice}}(X|\mu,\nu,t) =& \frac{1}{\sqrt{\pi}\sqrt{\sigma}} \times \left(\left\{ \sum_{l=-1}^{1} \sum_{k=-1}^{1} e^{-\frac{\left\{\sqrt{2}d[(k\mu+l\nu)\sinh(t)+(k\nu+l\mu)\cosh(t)]-X\right\}^2}{2\sigma}} \right. \right. \\
& \times \left[\mathrm{Re}\,(c_{k,l}) \cos\left(\frac{d^2A+\sqrt{2}XdC-X^2(\sinh(t)\nu+\cosh(t)\mu)}{B} \right) \right. \\
& \left. \left. -\mathrm{Im}\,(c_{k,l}) \sin\left(\frac{d^2A+\sqrt{2}XdC-X^2(\sinh(t)\nu+\cosh(t)\mu)}{B} \right) \right] \right\}^2 \\
& + \left\{ \sum_{l=-1}^{1} \sum_{k=-1}^{1} e^{-\frac{\left\{\sqrt{2}d[(k\mu+l\nu)\sinh(t)+(k\nu+l\mu)\cosh(t)]-X\right\}}{2\sigma}} \right. \\
& \times \left[\mathrm{Re}\,(c_{k,l}) \sin\left(\frac{d^2A+\sqrt{2}XdC-X^2(\sinh(t)\nu+\cosh(t)\mu)}{B} \right) \right. \\
& \left. \left. \left. +\mathrm{Im}\,(c_{k,l}) \cos\left(\frac{d^2A+\sqrt{2}XdC-X^2(\sinh(t)\nu+\cosh(t)\mu)}{B} \right) \right] \right\}^2 \right), \qquad (42)
\end{aligned}
$$

where

$$A = \frac{1}{2}\left[\sinh(3t)(3\mu^2+\nu^2)\nu(l^2-k^2) + \cosh(3t)(3\nu^2+\mu^2)\mu(l^2-k^2)\right.$$
$$\left. + \sinh(t)[(l^2-k^2)\nu + 4kl\mu](\nu^2-\mu^2) + \cosh(t)[(l^2-k^2)\mu + 4kl\nu](\nu^2-\mu^2)\right], \quad (43)$$
$$B = \cosh(3t)\nu(3\mu^2+\nu^2) + \sinh(3t)\mu(3\nu^2+\mu^2) + [\cosh(t)\nu + \sinh(t)\mu](\nu^2-\mu^2), \quad (44)$$
$$C = [k\sinh(2t) + l\cosh(2t)](\nu^2+\mu^2) + l(\nu^2-\mu^2) + 2[l\sinh(2t) + k\cosh(2t)]\mu\nu, \quad (45)$$
$$\sigma = \cosh(2t)(\mu^2+\nu^2) + 2\sinh(2t)\mu\nu. \quad (46)$$

As it was theoretically shown in Ref. [41], superpositions of coherent states, such as the one in Eq. (38), can be effectively used to approximate various quantum states of the harmonic oscillator, by determining the optimum distance d and coefficients c_{kl} of the superposition. The accuracy of the approximation can be characterized by the misfit parameter

$$\varepsilon = 1 - \left|\left\langle \psi_9^{\text{lattice}} \right| |\Psi\rangle\right|^2 H, \quad (47)$$

where the quantity $\left|\langle\psi_9^{\text{lattice}}||\Psi\rangle\right|^2$ is known as the fidelity between the target quantum state $|\Psi\rangle$ and the approximating coherent-state superposition $\left|\psi_9^{\text{lattice}}\right\rangle$. Using the misfit parameter as the objective function in a minimizing problem, one can determine the optimum values of d and c_{kl}. As it is a non-convex optimization problem of one real and nine complex parameters, an optimization algorithm supporting such problems has to be applied. In our calculations, we use the optimization method – the genetic algorithm of [42]. Note that the algorithm is stochastic and, as such, it has an inherent uncertainty. This can be suppressed by assuming high population sizes, choosing a high maximum number of iterations, and considering that the algorithm finds local minima, by repeating the optimization various times.

Table 1. Misfits and Optimum Parameters of the Approximations of Nonclassical States on a Lattice with 9 Coherent States. The Approximated States (Columns) Are Number State $|4\rangle$, Number State Superpositions $|\psi_{024}\rangle$ and $|\psi_{0123}\rangle$, and Amplitude Squeezed State $|\psi_{\text{AS}}(1,4,2)\rangle$. The Rows Show the Minimum Misfit ε, the Optimum Distances d_{opt}, and Complex Coefficients c_{kl} of the Approximation.

	$\|4\rangle$	$\|\psi_{024}\rangle$	$\|\psi_{0123}\rangle$	$\|\psi_{\text{AS}}(1,4,2)\rangle$
d_{opt}	1.375	0.703	0.544	0.838
$c_{-1,-1}$	$0.111+0.088i$	$0.606-0.708i$	$-0.370-0.465i$	$0.066-0.094i$
$c_{-1,0}$	$-0.687-0.550i$	$-0.219+0.107i$	$-0.217+0.160i$	$0.121+0.230i$
$c_{-1,1}$	$0.111+0.088i$	$0.600-0.769i$	$0.723-0.489i$	$-0.073-0.632i$
$c_{0,-1}$	$-0.687-0.550i$	$-0.888+0.923i$	$0.011+0.378i$	$-0.036+0.039i$
$c_{0,0}$	$1.000+0.801i$	$-0.316+0.508i$	$0.037-0.366i$	$-0.467-0.671i$
$c_{0,1}$	$-0.687-0.550i$	$-0.741+0.854i$	$-0.612-0.753i$	$0.893+0.999i$
$c_{1,-1}$	$0.111+0.088i$	$0.576-0.700i$	$-0.616+0.097i$	$-0.116+0.094i$
$c_{1,0}$	$-0.687-0.550i$	$-0.150+0.252i$	$0.414+0.313i$	$0.205+0.215i$
$c_{1,1}$	$0.111+0.088i$	$0.674-0.683i$	$0.148+0.891i$	$-0.616-0.122i$
ε	$1.321\cdot10^{-4}$	$1.244\cdot10^{-4}$	$4.983\cdot10^{-5}$	$5.436\cdot10^{-4}$

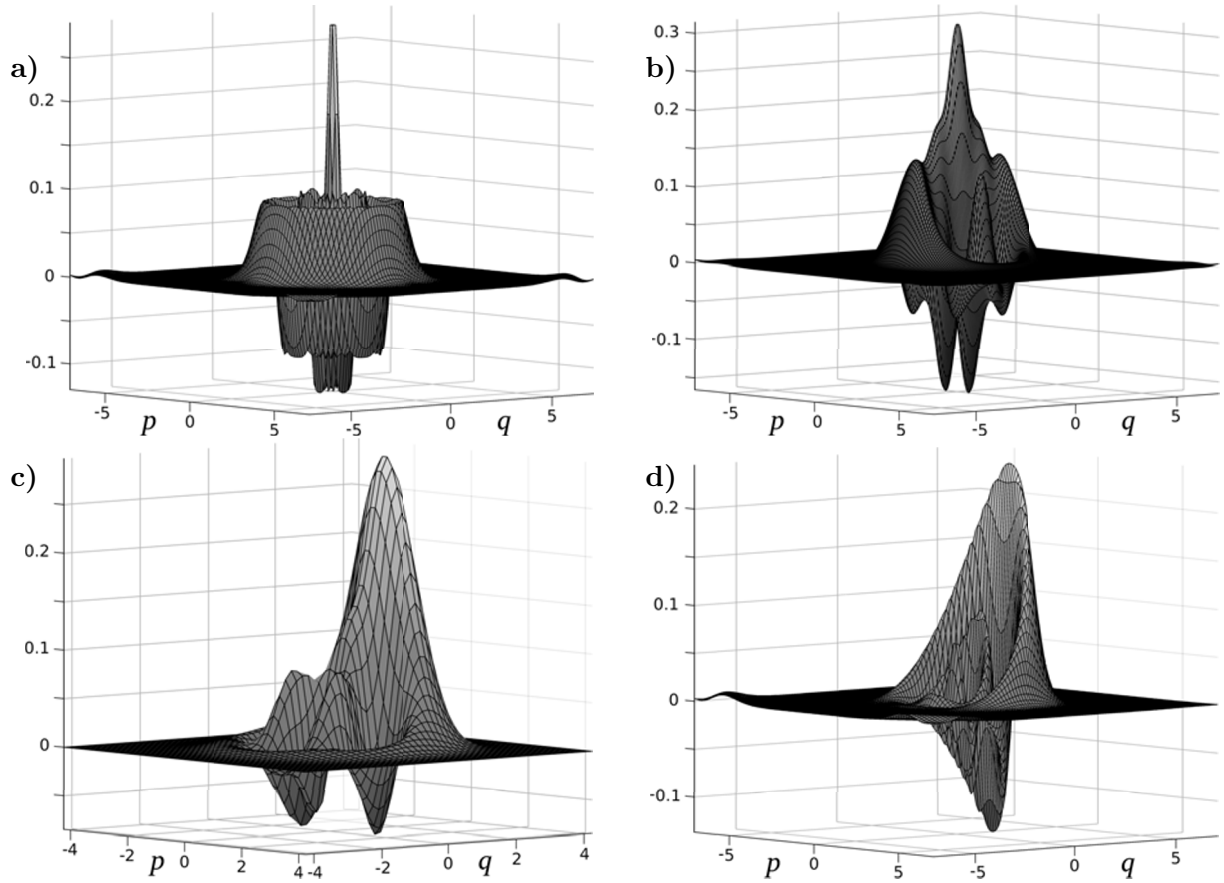

Fig. 1. Wigner functions of the superpositions of 9 coherent states on a 3×3 lattice in the phase space, approximating four nonclassical states; here, the number state $|4\rangle$ (a), the number state superposition $|\psi_{024}\rangle$ (b), the number state superposition $|\psi_{0123}\rangle$ (c), and the amplitude squeezed state $|\psi_{\rm AS}(1,4,2)\rangle$ (d).

Next, we present the superpositions of 9 coherent states on a 3×3 lattice in the phase space, approximating four nonclassical states. The considered nonclassical states are the number state $|4\rangle$ (a), the number state superpositions $|\psi_{024}\rangle = \frac{1}{\sqrt{3}}(|0\rangle + |2\rangle + |4\rangle)$ (b), $|\psi_{0123}\rangle = \frac{1}{2}(|0\rangle + |1\rangle + |2\rangle + |3\rangle)$ (c), and the amplitude squeezed state $|\psi_{\rm AS}(1,4,2)\rangle$ (d). The wave functions of the number state and the superpositions of the number states are

$$\psi_4(x) = \frac{1}{4\sqrt{\sqrt{\pi}4!}} \exp(-x^2/2) H_4(x), \tag{48}$$

$$\psi_{024}(x) = \frac{1}{\sqrt{3}} \left[\sum_{k=0}^{2} \frac{1}{2^k \sqrt{\sqrt{\pi}(2k)!}} \exp(-x^2/2) H_{2k}(x) \right], \tag{49}$$

$$\psi_{0123} = \frac{1}{2} \left[\sum_{n=0}^{3} \frac{1}{\sqrt{2^n \sqrt{\pi} n!}} \exp(-x^2/2) H_n(x) \right]. \tag{50}$$

Amplitude squeezed states read

$$|\psi_{\rm AS}(u,\delta,R)\rangle = \mathcal{N}\int_{-\pi}^{\pi} \exp(-\frac{1}{2}u^2\phi^2 - i\delta\phi)\Big|Re^{i\phi}\Big\rangle \,{\rm d}\phi, \tag{51}$$

being defined by Gaussian continuous coherent-state superpositions in the phase space, where $\mathcal{N}$ is a normalization constant. These states tend to the coherent state R in the limit $u \to \infty$ and yield the photon number state δ, when δ is a nonnegative integer in the limit $u \to 0$, while at $\delta = R^2$, the mean values of the photon number for these limiting states are equal. To analytically calculate the wave function of these states is nontrivial, and explicit wave function is not known in the literature. Consequently, the explicit exact symplectic tomogram deduced from Eq. (6) cannot be determined; therefore, the approximate tomogram presented in Eq. (41) becomes useful.

First, using the methods described above, we determine the parameters of the coherent state superpositions of 9 coherent states on a 3×3 lattice in the phase space by approximating these states. The results are presented in Table 1, where the optimum parameters d and c_{kl} of the approximations are shown along with the minimum misfits ε. In Fig. 1, we show the Wigner functions of the four approximating superpositions. The Wigner functions are calculated by substituting the approximating wave function (39) into Eq. (9). Also, we checked that the same result could be obtained by inserting the approximating tomogram (40) into Eq. (11). In addition, we calculated the Wigner functions of the target states and found that the difference between the Wigner functions of the target states and the approximating states are smaller than 10^{-3} for all the points in the phase space. Hence, generic symplectic tomogram defined in Eq. (41) can be used to describe several nonclassical states.

4. Discussion

We determined the evolving symplectic tomograms of several important nonclassical states of the inverted oscillator, by applying the method of integrals of motion developed in Ref. [23,33] for this system. We considered even and odd Schrödinger cat states, squeezed coherent states, and lattice superpositions of coherent states initially prepared in the potential of harmonic oscillator. In the case of the inverted oscillator, the position $\hat{q}_H(t)$ and momentum $\hat{p}_H(t)$ operators in the Heisenberg representation are given as the integrals of motion, and they are linear in the position and momentum operators in the Schrödinger picture. Hence, evolving symplectic tomograms of the inverted oscillator can be found by a corresponding time-dependent transformation of the parameters of the initial tomograms. The significance of the lattice superpositions of coherent states is that they can approximate several nonclassical states with high precision. We note that, in the case of multi-mode oscillators, superpositions of states can be entangled. Tomograms of entangled states are entangled probability distributions [34]; they have not been studied in the classical probability theory, and their properties can be studied, in view of the approach developed above. Using lattice superpositions, we provided explicit results for the approximation of number states, photon number superpositions, and amplitude squeezed states, by determining the parameters of the superpositions also appearing in the approximating probability representation. Also, we calculated the Wigner functions of the considered target states and found that the difference between the Wigner functions of the target states and the approximating states are negligible for all the points in the phase space. Hence, the lattice superpositions of coherent states and their probability representation can be effectively used for describing various nonclassical states of the inverted oscillators.

Acknowledgments

This research was funded by the National Research, Development and Innovation Office, Hungary under Grants Nos. TKP2021-NVA-04 and TKP2021-EGA-17.

References

1. S. Mancini, V. I. Man'ko, and P. Tombesi, *Phys. Lett. A*, **213**, 1 (1996); DOI: 10.1016/0375-9601(96)00107-7
2. A. Ibort, V. I. Man'ko, G. Marmo, et al., *Phys. Scr.*, **79**, 65013 (2009); DOI: 10.1088/0031-8949/79/06/065013
3. G. G. Amosov, Y. A. Korennoy, and V. I. Man'ko, *Phys. Rev. A*, **85**, 052119 (2012); DOI: 10.1103/PhysRevA.85.052119
4. M. Asorey, A. Ibort, G. Marmo, and F. Ventriglia, *Phys. Scr.*, **90**, 074031 (2015); DOI: 10.1088/0031-8949/90/7/074031
5. O. V. Man'ko and V. I. Man'ko, *Entropy*, **23**, 549 (2021); DOI: 10.3390/e23050549
6. E. Wigner, *Phys. Rev.*, **40**, 749 (1932); DOI: 10.1103/PhysRev.40.749
7. K. Husimi, *Proc. Phys.-Math. Soc. Jpn.*, **22**, 264 (1940); DOI: 10.11429/ppmsj1919.22.4_264
8. Y. Kano, *J. Math. Phys.*, **6**, 1913 (1965); DOI: 10.1063/1.1704739
9. R. J. Glauber, *Phys. Rev. Lett.*, **10**, 84 (1963); DOI: 10.1103/PhysRevLett.10.84
10. E. C. G. Sudarshan, *Phys. Rev. Lett.*, **10**, 277 (1963); DOI: 10.1103/PhysRevLett.10.277
11. V. I. Man'ko and L. A. Markovich, *J. Math. Phys.*, **61**, 102102 (2020); DOI: 10.1063/5.0019203
12. V. Dodonov and V. Man'ko, *Phys. Lett. A*, **229**, 335 (1997); DOI: 10.1016/S0375-9601(97)00199-0
13. V. I. Man'ko and O. V. Man'ko, *J. Exp. Theor. Phys.*, **85**, 430 (1997); DOI: 10.1134/1.558326
14. M. O. T. Cunha, V. I. Man'ko, and M. O. Scully, *Found. Phys. Lett.*, **14**, 103 (2001); DOI: 10.1023/A:1012373419313
15. G. M. D'Ariano, L. Maccone, and M. Paini, *J. Opt. B: Quantum Semiclass. Opt.*, **5**, 77 (2003); DOI: 10.1088/1464-4266/5/1/311
16. P. Adam, V. A. Andreev, I. Ghiu, et al., *J. Russ. Laser Res.*, **35**, 3 (2014); DOI: 10.1007/s10946-014-9395-6
17. P. Adam, V. A. Andreev, M. A. Man'ko, and V. I. Man'ko, *J. Russ. Laser Res.*, **38**, 491 (2017); DOI: 10.1007/s10946-017-9673-1
18. V. N. Chernega, O. V. Man'ko, and V. I. Man'ko, *J. Russ. Laser Res.*, **38**, 324 (2017); DOI: 10.1007/s10946-017-9648-2
19. P. Adam, V. A. Andreev, M. A. Man'ko, et al., *J. Russ. Laser Res.*, **41**, 470 (2020); DOI: 10.1007/s10946-020-09900-x
20. P. Adam, V. A. Andreev, M. A. Man'ko, et al., *Symmetry*, **12**, 1099 (2020); DOI: 10.3390/sym12071099
21. P. Adam, V. A. Andreev, M. A. Man'ko, et al., *Symmetry*, **13**, 131 (2021); DOI: 10.3390/sym13010131
22. O. V. Man'ko, V. I. Man'ko, and G. Marmo, *J. Phys. A: Math. Gen.*, **35**, 699 (2002); DOI: 10.1088/0305-4470/35/3/315
23. M. A. Man'ko and V. I. Man'ko, *Entropy*, **25**, 213 (2023); DOI: 10.3390/e25020213
24. P. Adam, M. A. Man'ko, and V. I. Man'ko, *J. Russ. Laser Res.*, **43**, 1 (2022); DOI: 10.1007/s10946-022-10030-9
25. V. Dodonov, I. Malkin, and V. Man'ko, *Physica*, **72**, 597 (1974); DOI: 10.1016/0031-8914(74)90215-8
26. F. Ullinger, M. Zimmermann, and W. P. Schleich, *AVS Quantum Sci.*, **4**, 024402 (2022); DOI: 10.1116/5.0074429
27. V. Subramanyan, S. S. Hegde, S. Vishveshwara, and B. Bradlyn, *Ann. Phys.*, **435**, 168470 (2021); DOI: 10.1016/j.aop.2021.168470
28. D. J. Cirilo-Lombardo and N. G. Sanchez, *Phys. Rev. D*, **108**, 126001 (2023); DOI: 10.1103/PhysRevD.108.126001

29. W. Wöger, H. King, R. J. Glauber, and J. W. Haus, *Phys. Rev. A*, **34**, 4859 (1986); DOI: 10.1103/PhysRevA.34.4859
30. A. Vourdas and R. F. Bishop, *J. Phys. A: Math. Gen.*, **31**, 8563 (1998); DOI: 10.1088/0305-4470/31/42/015
31. C. Yuce, A. Kilic, and A. Coruh, *Phys. Scr.*, **74**, 114 (2006); DOI: 10.1088/0031-8949/74/1/014
32. C. Yuce, *Phys. Scr.*, **96**, 105006 (2021); DOI: 10.1088/1402-4896/ac1087
33. O. V. Man'ko and V. I. Man'ko, *Entropy*, **25**, 217 (2023); DOI: 10.3390/e25020217
34. V. N. Chernega and O. V. Man'ko, *Entropy*, **25**, 785 (2023); DOI: 10.3390/e25050785
35. J. Radon, *Verh. Sachs. Akad. Wiss. Leipzig, Math. Phys. Klass.*, **69**, 262 (1917).
36. D. T. Smithey, M. Beck, M. G. Raymer, and A. Faridani, *Phys. Rev. Lett.*, **70**, 1244 (1993); DOI: 10.1103/PhysRevLett.70.1244
37. V. V. Dodonov, I. A. Malkin, and V. I. Man'ko, *J. Phys. A: Math. Gen.*, **8**, L19 (1975); DOI: 10.1088/0305-4470/8/2/001
38. J. Bertrand and P. Bertrand, *Found. Phys.*, **17**, 397 (1987); DOI: 10.1007/BF00733376
39. K. Vogel and H. Risken, *Phys. Rev. A*, **40**, 2847 (1989); DOI: 10.1103/PhysRevA.40.2847
40. E. Munguá-González, S. Rego, and J. K. Freericks, *Am. J. Phys.*, **89**, 885 (2021); DOI: 10.1119/10.0004872
41. P. Adam, E. Molnar, G. Mogyorosi, et al., *Phys. Scripta*, **90**, 074021 (2015); DOI: 10.1088/0031-8949/90/7/074021
42. D. Goldberg, *Genetic Algorithms in Search, Optimization, and Machine Learning*, Addison-Wesley (1989).